Exchange bias and blocking temperature distribution of Fe-film/CoO-nanoparticle hybrid bilayers

Wei Zhang and Kannan M. Krishnan

Citation: Journal of Applied Physics **115**, 17D714 (2014); doi: 10.1063/1.4865215
View online: http://dx.doi.org/10.1063/1.4865215
View Table of Contents: http://scitation.aip.org/content/aip/journal/jap/115/17?ver=pdfcov
Published by the AIP Publishing

Exchange bias and blocking temperature distribution of Fe-film/CoO-nanoparticle hybrid bilayers

Wei Zhang[a] and Kannan M. Krishnan[b]
Department of Materials Science and Engineering, University of Washington, Seattle, Washington 98195, USA

(Presented 5 November 2013; received 23 August 2013; accepted 7 November 2013; published online 12 February 2014)

We fabricated and characterized Fe-film/CoO-nanoparticle hybrid bilayers and studied their temperature-dependent magnetic properties. The magnetic nanoparticles are uncoupled or weakly coupled in the particle films, which essentially resemble the antiferromagnetic grains in the deposited thin films. The size and size distribution of the nanoparticles can be well-controlled by chemical synthesis prior to assembling, providing additional route for engineering the antiferromagnetic layer in exchange-bias systems. Using cycled annealing-cooling measurements, we observed a unimodal blocking-temperature distribution in our samples that is a reflection of the intrinsic antiferromagnetic monodisperse "grain" size distribution. The absence of the low-temperature contribution is likely attributed to both the fabrication process and the nanoparticle morphology. © *2014 AIP Publishing LLC*. [http://dx.doi.org/10.1063/1.4865215]

The ferromagnetic (F)/antiferromagnetic (AF) interaction leading to the exchange bias (EB) effect,[1] is central to the design and operation of practical spintronics devices. The EB effect manifests itself as a unidirectional pinning of the F magnetization.[2] Single-crystal, thin-film F/AF bilayers,[3,4] have been studied to reveal EB properties including competing anisotropies,[5,6] individual spin behaviors,[7,8] and collective long-range effects.[9,10] On the other hand, the need for miniaturization further motivates research into nanostructures, which can be achieved by either epitaxial patterning of thin films[11–13] or chemical synthesis of nanoparticles (NPs).[14–16] Although plenty of work has been done to explore the EB effect within the respective thin-film or NP morphologies, less has been done to understand the magnetic properties of thin films coupled to NP arrays.[17,18]

Recently, the gap in understanding EB in hybrid thin film and NP systems has been theoretically bridged by an enlightening model for EB.[19] Specifically, the AF layer is viewed as an assembly of almost exchange-decoupled grains, having pinning energy KV, where K is the AF anisotropy energy per unit volume and V is the grain volume. Therefore, hybrid EB bilayers with the AF layer being chemically synthesized NPs may bring new pathways for tailoring their EB properties due to their controllable size and size distribution. Such distribution of grain size further gives rise to the distribution of blocking temperature, T_B. The "T_B-distribution" technique has been widely used in evaluating thin-film samples[20–24] but has not been reported in any hybrid bilayers, in which the effect from the grain size distribution may be more significant.

We fabricated CoO-NPs/Fe-film hybrid bilayers with the following recipe: Co NPs (10 nm in diameter and with a narrow size distribution) were chemically synthesized by a thermal decomposition method.[25,26] Co-NP films, a few layers thick, were obtained by assembling these chemically synthesized Co NPs on clean Si substrates via a controlled solvent evaporation technique.[26] The NP films were then annealed at 400 °C under a continuous O_2 flow in a tube furnace for 1.5 h to convert the Co NPs to Co-oxide. Finally, we deposited a 30 nm Fe-film followed by a 5 nm Ta cap, by ion beam sputtering at a base pressure $\sim 1 \times 10^{-7}$ Torr on top of the Co-oxide NP film. The surface composition was examined by energy dispersive x-ray spectroscopy (EDS) at each step during the above process. After assembling the NPs, C, O, and Co peaks were co-observed (Fig. 1(a)) in which the C peak is due to the chemical residue from the chemical synthesis. After the O-rich annealing, the C peak was

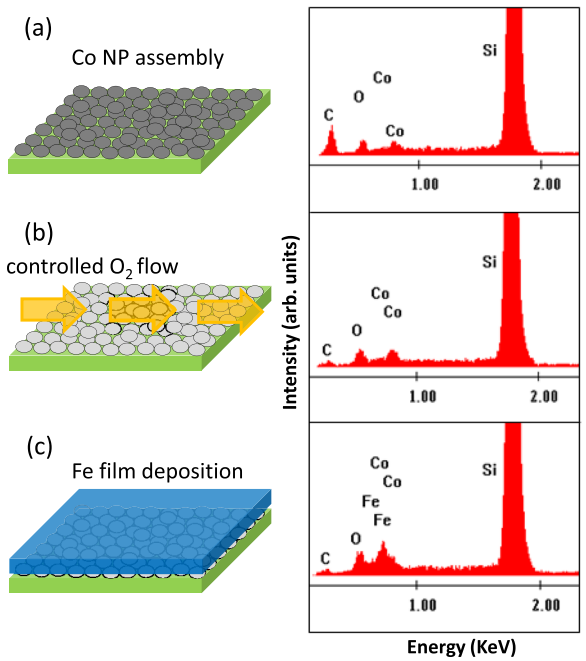

FIG. 1. Illustration of the sample fabrication process and corresponding energy-dispersive x-ray spectrum at each critical step.

[a]Present address: Materials Science Division, Argonne National Laboratory, Lemont, IL 60439, USA.
[b]Author to whom correspondence should be addressed. Electronic mail: kannanmk@uw.edu

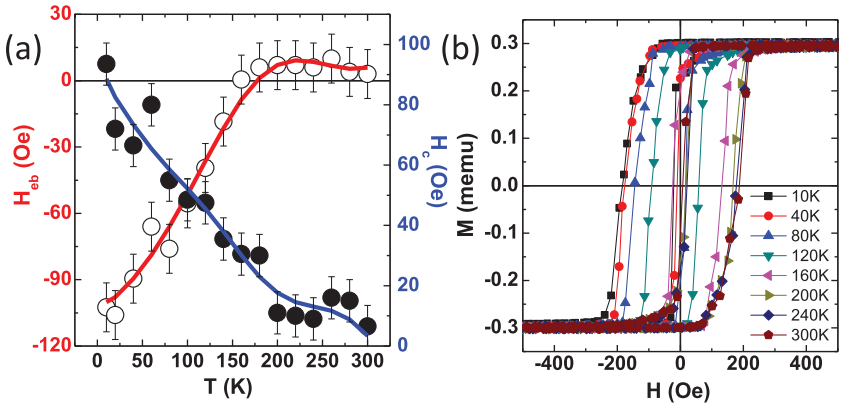

FIG. 2. (a) Temperature dependence of the coercivity $H_c(T)$, and the bias field $H_{eb}(T)$, obtained by measuring hysteresis loops at temperatures from 10 to 300 K. (b) Hysteresis loops measured for different annealing temperatures (T_a). The loops were all recorded at 10 K along the FC direction.

significantly reduced (Fig. 1(b)) primarily due to the conversion of C to CO_2. On the other hand, Co NPs were fully converted to CoO_x due to the large surface-to-volume ratio of the NPs. Finally, after depositing the Fe layer, a strong Fe peak was detected in the EDS spectrum (Fig. 1(c)).

Hysteresis loops at various temperatures from 10 to 300 K were measured, and the temperature dependence of the coercivity, $H_c(T)$, and the bias field, $H_{eb}(T)$ are summarized in Fig. 2. Field cooling (FC) from 380 K down to 10 K under a magnetic field, $H_{FC} = 10$ kOe was first applied to set the EB. Hysteresis loops were then measured on increasing temperature. From the $H_{eb}(T)$ curve, the T_B is determined to be $\sim$160 K. For $T < 160$ K, the loops exhibit a negative shift from the origin due to the exchange coupling between Fe and the ordered CoO phase. For $T > 160$ K (CoO disordered), the loop-shift, instead of vanishing to zero, actually switched to the same direction as H_{FC}, which indicates an unconventional positive EB and its magnitude, $H_{eb} \sim 8$ Oe, remains roughly unchanged above 160 K.

To study the intrinsic AF-grain effect on the T_B-distribution, we applied a special measurement as described in Ref. 20. The sample was initially cooled at $H_{FC} = 10$ kOe from 380 K down to 10 K. Following the initial FC, T_B-distribution in the range of 10 K to 380 K is deduced from the hysteresis loop measurements (Fig. 2(b)).

The T_a-dependent coercivity, $H_c(T_a)$ and bias field, $H_{eb}(T_a)$ were subsequently determined from the loops, and are summarized in Fig. 3(b). $H_{eb}(T_a)$ curve exhibits a strong dependence, with a EB sign change at $\sim$150 K and a saturation around 220 K. The derivative of $H_{eb}(T_a)$ vs T_a, i.e., $\delta H_{eb}(T_a)/\delta T_a$, actually represents the T_B distribution of the sample.[20–24] Earlier works on continuous thin-film samples all suggested a bimodal distribution, where two peaks in the $\delta H_{eb}(T_a)/\delta T_a$ curve were observed.[20] However, only the high-T peak is directly related to the grain size distribution, while the sharp increase at low-T is attributed to the spin-glass contribution. The grain size distribution in EB thin-film samples has been systematically revealed in Ref. 19. Most AF grains are in the size $\sim$5–7 nm; and increasing the AF thickness only slightly enhances the grain size. The surface spins of these small grains give rise to high frustration; thus, a gradual freezing of the interfacial frustrated spins can explain the observation of the sharp increase at low-T in the $\delta H_{eb}(T_a)/\delta T_a$ curve.

The T_B-distribution of our hybrid bilayer is shown in Fig. 3(b). Unlike that reported for thin-film samples, the $\delta H_{eb}(T_a)/\delta T_a$ curve indicates a unimodal T_B-distribution which reflects the intrinsic grain size distribution of the AF layer. The absence of the low-T peak is likely due to the sample fabrication process. In the previously reported

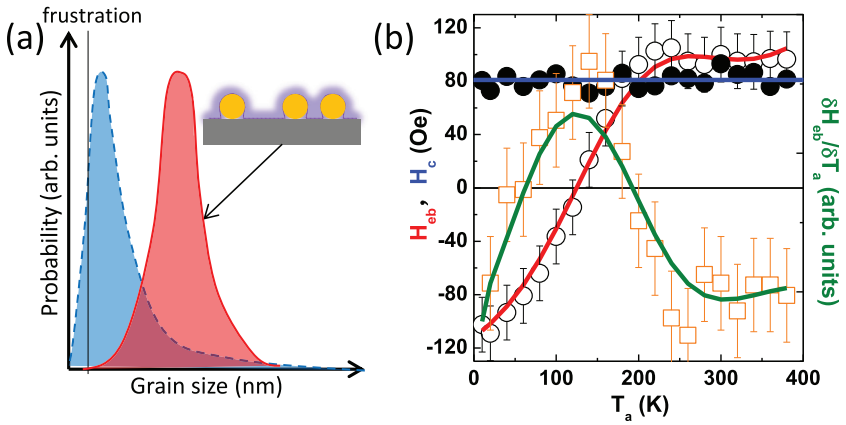

FIG. 3. (a) Schematic illustration of the grain size and size distribution of thin-film (dashed) and assembled NP-film (solid) samples. The dashed curve is a schematic representation of the experimental curves obtained from Ref. 19, where most grains are less than 10 nm in size including small/incomplete grains that likely contribute to the spin-glass regions. The solid curve is a schematic representation of the NPs used in this work, with an average size of $\sim$10 nm and a narrow size distribution (Ref. 26). The inset figure illustrates the core-shell-like microstructures at the interface (Ref. 17). (b) Dependence of the coercivity H_c, EB field H_{eb}, and derivative $\delta\delta H_{eb}(T_a)/\delta T_a$ on the annealing temperature (T_a).

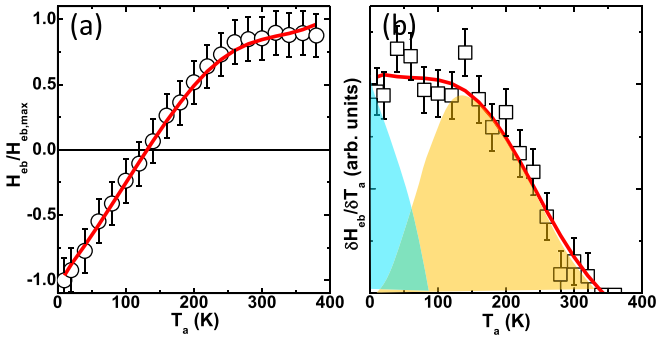

FIG. 4. Dependence of (a) EB field H_{eb}, and (b) derivative $\delta H_{eb}(T_a)/\delta T_a$ on the annealing temperature (T_a) for the thin-film reference sample.

thin-film samples,[20–24] both the F and AF layers were deposited *in situ* and also subjected to post thermal annealing at $T \geq 450$ K. The interfacial intermixing is inevitable during the initial establishment (growth) of the interface and also during the post-annealing. In our hybrid samples, the AF layer (NP-film) is fabricated *ex situ* by NP assembly and oxidation; only the F layer is deposited in a vacuum chamber. As a result, the intermixing between NPs and post-deposited Fe layer is minimized. In addition, the microstructure at the interface also plays an important role in the hybrid samples. Due to the NP-film morphology, the deposited Fe layer would form localized CoO/Fe core-shell-like structures (inset of Fig. 3(a)). Such morphology has also been confirmed by transmission-electron microscopy observation.[17] Consequently, the magnetic properties are largely determined by the intrinsic size and size distribution of the NPs. Engineering of the NP-films for optimized properties will become an important aspect for such hybrid systems in the future.

We also fabricated a reference sample in which the F and AF layers were both made by *in situ* physical deposition. The sample structure is CoO(4 nm)/Fe(30 nm)/Ta(5 nm). Similar measurements were performed and the $H_{eb}(T_a)$ and $\delta H_{eb}(T_a)/\delta T_a$ curves are shown in Fig. 4. Specifically, the $\delta H_{eb}(T_a)/\delta T_a$ shows a single broad plateau (Fig. 4(b)), which is the result of the overlap of the high-T and low-T peaks. The high-T peak is related to the AF grain distribution, taking into account not only the grains at the F/AF interface but also in its bulk. The T_B-distribution is thus directly related to the grain size distribution. On the other hand, the low-T peak comes from the spin-glass phase, in which the frustrated spins always undergo spin reorganization instead of being set along H_{FC}.

This work was supported by NSF-DMR under Grant No. #1063489. We thank T. Wen for fruitful discussions.

[1]W. H. Meiklejohn and C. P. Bean, Phys. Rev. **105**, 904 (1957).
[2]J. Nogues and I. K. Schuller, J. Magn. Magn. Mater. **192**, 203 (1999).
[3]W. Zhang *et al.*, Appl. Phys. Lett. **98**, 092503 (2011).
[4]Q. Zhan *et al.*, Phys. Rev. B **83**, 094404 (2011).
[5]W. Zhang and K. M. Krishnan, J. Magn. Magn. Mater. **324**, 3129 (2012).
[6]W. Zhang and K. M. Krishnan, J. Appl. Phys. **111**, 07D712 (2012).
[7]S. Bruck *et al.*, Phys. Rev. Lett. **101**, 126402 (2008).
[8]S. Roy *et al.*, Phys. Rev. Lett. **95**, 047201 (2005).
[9]W. Zhang and K. M. Krishnan, Phys. Rev. B **86**, 054415 (2012).
[10]W. Zhang and K. M. Krishnan, Phys. Rev. B **88**, 024428 (2013).
[11]W. Zhang *et al.*, J. Micromech. Microeng. **21**, 045024 (2011).
[12]W. Zhang *et al.*, J. Appl. Phys. **113**, 17B502 (2013).
[13]W. Zhang *et al.*, J. Appl. Phys. **107**, 09D724 (2010).
[14]G. Salazar-Alvarez *et al.*, J. Am. Chem. Soc. **129**, 9102 (2007).
[15]A. E. Berkowitz *et al.*, Phys. Rev. B **77**, 024403 (2008).
[16]D. W. Kavich *et al.*, Phys. Rev. B **78**, 174414 (2008).
[17]S. Thomas *et al.*, Nanotechnology **24**, 155703 (2013).
[18]W. Zhang *et al.*, Appl. Phys. Lett. **101**, 132401 (2012).
[19]K. O'Grady *et al.*, J. Magn. Magn. Mater. **322**, 883 (2010).
[20]V. Baltz *et al.*, Phys. Rev. B **81**, 052404 (2010).
[21]V. Baltz *et al.*, Appl. Phys. Lett. **96**, 262505 (2010).
[22]V. Baltz and B. Dieny, J. Appl. Phys. **109**, 066102 (2011).
[23]C. K. Safeer *et al.*, Appl. Phys. Lett. **100**, 072402 (2012).
[24]K. Akmaldinov *et al.*, Appl. Phys. Lett. **103**, 042415 (2013).
[25]V. F. Puntes *et al.*, Science **291**, 2115 (2001).
[26]T. Wen and K. M. Krishnan, J. Phys. D: Appl. Phys. **44**, 393001 (2011).